

Spectroscopic and Density Functional Theory Studies of the Molecular Geometry and Electronic Structure of Classical and Nonclassical Radical Ions Derived from 7-Benzhydrylidenenorbornene Analogues

Hayato Namai,[†] Hiroshi Ikeda,^{*,‡} Takashi Hirano,[§] Hideki Ishii,[§] and Kazuhiko Mizuno[‡]

Department of Chemistry, Graduate School of Science, Tohoku University, Sendai 980-8578, Japan, Department of Applied Chemistry, Graduate School of Engineering, Osaka Prefecture University, Sakai, Osaka 599-8531, Japan, and Department of Applied Physics and Chemistry, The University of Electro-Communications, Chofu, Tokyo 182-8585, Japan

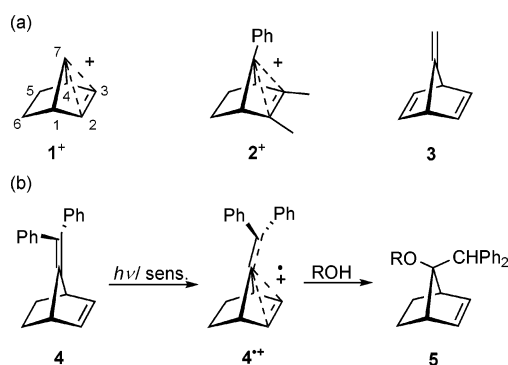
Received: December 30, 2006; In Final Form: April 28, 2007

A spectroscopic study, using nanosecond time-resolved laser flash photolysis and γ -irradiation of low-temperature matrices, was undertaken along with a theoretical study using density functional theory (DFT) and time-dependent (TD)-DFT calculations to gain insight into the molecular geometry and electronic structure of radical cations and radical anions of 7-benzhydrylidenenorbornene (**4**) and its derivatives **6–8**. The radical ions **4**^{•+}, **6**^{•+}, **7**^{•+}, **8**^{•+}, **4**^{•-}, **6**^{•-}, **7**^{•-}, and **8**^{•-} exhibited clear absorption bands in the 350–800 nm region, which were reproduced successfully from the electronic transitions calculated with TD-UB3LYP/cc-pVDZ. Radical cations **4**^{•+} and **8**^{•+} are consistent with a bent structure having a delocalized electronic state where the spin and charge are delocalized not only in the benzhydrylidene subunit but also in the residual subunit. In contrast, **6**^{•+} and **7**^{•+} have nonbent structures with a localized electronic state where their spin and charge are localized in the benzhydrylidene subunit only. Therefore, **4**^{•+} and **8**^{•+} have a nonclassical nature, with **6**^{•+} and **7**^{•+} possessing a classical nature. In contrast, in the radical anion system, **7**^{•-} and **8**^{•-} are considered nonclassical, and **4**^{•-} and **6**^{•-} are classical. Orbital interaction theory and DFT calculations can account fully for the spectroscopic features, molecular geometries, and electronic structures of the radical ions. For example, the shift of the absorption bands and the nonclassical nature of **4**^{•+} are due to the antibonding character of the highest occupied molecular orbital (HOMO) of **4**, and those of **7**^{•-} arise from the bonding character of the lowest unoccupied molecular orbital (LUMO) of **7**. A topological agreement of *p*-orbitals at C-2, C-3 (or C-5, C-6), and C-7 produces strong electronic coupling with an antibonding or a bonding character in the frontier orbitals. It is the ethylene and butadiene skeleton at C-2–C-3 (or C-5–C-6), with its contrasting topology in the HOMO and LUMO of the neutral precursor, that holds the key to deducing the nonclassical nature of the 7-benzhydrylidenenorbornene-type radical cation and radical anion systems.

Introduction

The 7-norbornenyl cation (**1**⁺, Scheme 1), with its bent structure and delocalized cationic center, ranks as a prototype of nonclassical cations.¹ A variety of experimental and theoretical investigations over several decades have examined² its distinctive molecular geometry and electronic structure, with its extraordinary reactivity attracting the attention of many chemists.^{3–7} Recently, X-ray structural analysis of the 2,3-dimethyl-7-phenyl-7-norbornenyl cation (**2**⁺) and derivatives by Laube⁸ has provided conclusive proof that, at least in the solid state, the 7-norbornenyl-type cation has a three-center, two-electron bond in a bent structure, i.e., a symmetrical delocalized structure. By analogy with **1**⁺, any radical cation of 7-methylenenorbornadiene (**3**) should possess homoconjugation between three olefinic parts to stabilize its radical cation center. Roth et al. proposed that homoconjugation played a crucial role in stabilizing **3**^{•+}^{9a} in the course of their analysis using chemically induced dynamic nuclear polarization (CIDNP).^{9b} Their work

SCHEME 1: (a) Nonclassical Cations (**1**⁺ and **2**⁺) and Related Compound (**3**) and (b) the π -Facial Selective Nucleophilic Addition of ROH to **4**^{•+} Induced by the PET Reaction of **4**^a



^a Abbreviations: sens. = sensitizer; R = Me or H.

is the sole study of homoconjugation in radical cations of 7-methylenenorbornene analogues.

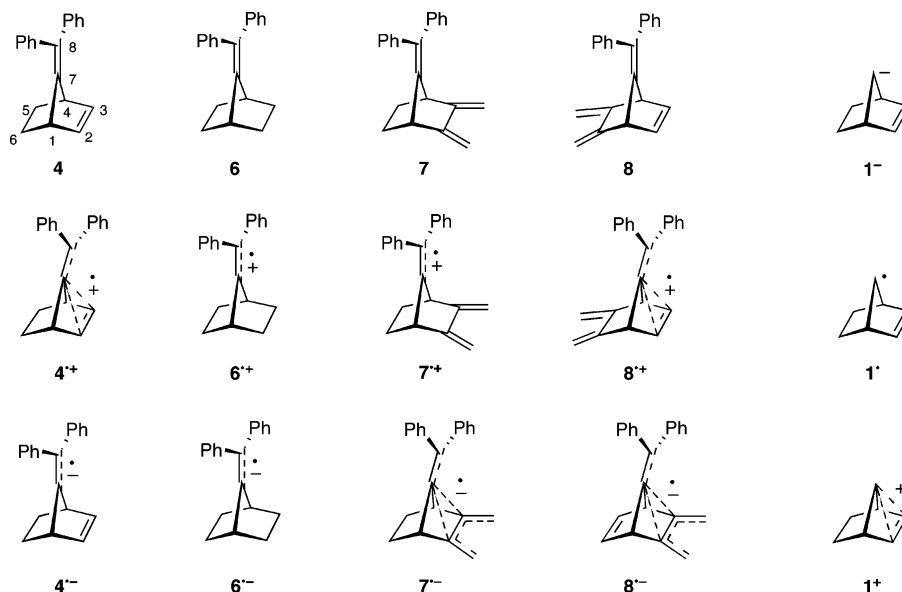
A comparison of experimental UV/vis absorption spectroscopy with the calculated absorption spectra for these radical cations can provide insight into the molecular geometry and

* To whom correspondence should be addressed. E-mail: ikeda@chem.osakafu-u.ac.jp

[†] Tohoku University (TU).

[‡] Osaka Prefecture University (OPU).

[§] The University of Electro-Communications (UEC).

CHART 1: 7-Benzhydrylidenebornene Derivatives (4 and 6–8), the Corresponding Radical Cations ($4^{+\bullet}$ and $6^{+\bullet}$ – $8^{+\bullet}$), the Corresponding Radical Anions ($4^{-\bullet}$ and $6^{-\bullet}$ – $8^{-\bullet}$), and Related Intermediates (1^- , 1^{\bullet} , and 1^+)

electronic structure involved in homoconjugation. We have undertaken such an analysis, focusing on electron-transfer reactions of 7-benzhydrylidenebornene (**4**,¹⁰ Scheme 1). Because the substitution of two phenyl groups in **4** induces lowering of the oxidation potential and an increase in the HOMO, phenyl substitutions make it easy to generate and observe the relevant $4^{+\bullet}$ absorption band in the visible region using electron-transfer reactions coupled with UV/vis absorption spectroscopy. The reactivity of $4^{+\bullet}$ was the subject of a study by Hirano and Ohashi.¹¹ The radical ion $4^{+\bullet}$ was generated by a photoinduced electron transfer (PET) that induced π -facially selective nucleophilic addition of MeOH or H₂O to yield **5**. The authors argued that this resulted from the formation of a nonclassical radical cation¹² ($4^{+\bullet}$) with homoconjugative electronic coupling¹³ among C-2, C-3, and C-7 in a single-minimum potential surface. It would be advantageous to know whether nonclassical *radical anions*, counterparts of the nonclassical *radical cations*, are generated by the injection of an electron into the same precursors.

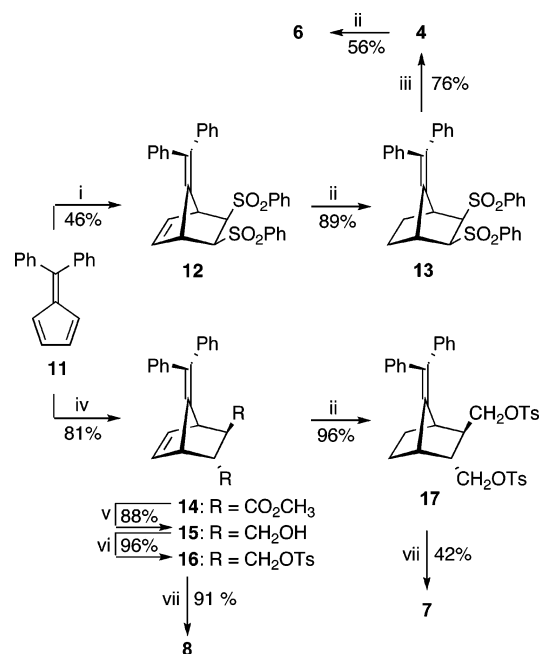
In our study, we compared calculations from density functional theory (DFT) with UV/vis absorption spectra of the radical cations of **4**, 7-benzhydrylidenebornane (**6**, Chart 1), 7-benzhydrylidene-2,3-dimethylenenorbornane (**7**), and 7-benzhydrylidene-5,6-dimethylenenorbornane (**8**), obtained using nano-second time-resolved laser flash photolysis (LFP). We also compared the UV/vis absorption spectra of γ -irradiated low-temperature matrices of **4**, **6**, **7**, and **8** with DFT calculations of their radical anions, i.e., the counterparts of the radical cations $4^{+\bullet}$, $6^{+\bullet}$, $7^{+\bullet}$, and $8^{+\bullet}$. As a result, we were able to deduce the molecular geometry and electronic structure of both the radical cations and radical anions of **4**, **6**, **7**, and **8**, and to demonstrate that their classical and nonclassical natures are controlled topologically.¹⁵

Experimental Section

General Method. See the Supporting Information for details.

Preparation of 4, 6, 7, and 8. 7-Benzhydrylidenebornene (**4**)¹⁶ and its derivatives **6–8** were prepared using the procedure shown in Scheme 2. The norbornane derivative (**13**) was prepared by the Diels–Alder reaction of diphenylfulvene (**11**) with (*Z*)-1,2-bis(phenylsulfonyl)ethene followed by regioselective

SCHEME 2: Reagents and Conditions: (i) (*Z*)-1,2-Bis(phenylsulfonyl)ethene, Toluene Reflux; (ii) H₂, Pd–C; (iii) 3% Na–Hg, NaH₂PO₄, CH₃OH; (iv) Dimethyl Fumarate, Benzene Reflux; (v) LiAlH₄, Ether; (vi) Tosyl Chloride (TsCl), Pyridine; (vii) *t*-BuOK, DMSO



hydrogenation of the norbornene derivative (**12**). The reductive elimination reaction¹⁶ of **13** gave **4**, which was converted into **6** using similar regioselective hydrogenation. An alternative norbornane derivative (**17**) was prepared by the Diels–Alder reaction of **11** with dimethyl fumarate followed by reduction, tosylation, and hydrogenation via norbornene intermediates (**14–16**). Norbornanes **16** and **17** were converted into **8** and **7**, respectively. See the Supporting Information for details.

Nanosecond Time-Resolved UV/Vis Absorption Spectroscopy on Laser Flash Photolysis. A sample solution (2 mL) of acetonitrile containing the substrate (1 mM), *N*-methylquinolinium tetrafluoroborate (NMQ⁺BF₄⁻) (10 mM) as a sensitizer, and toluene (1 M) as a cosensitizer in a glass cell was prepared.

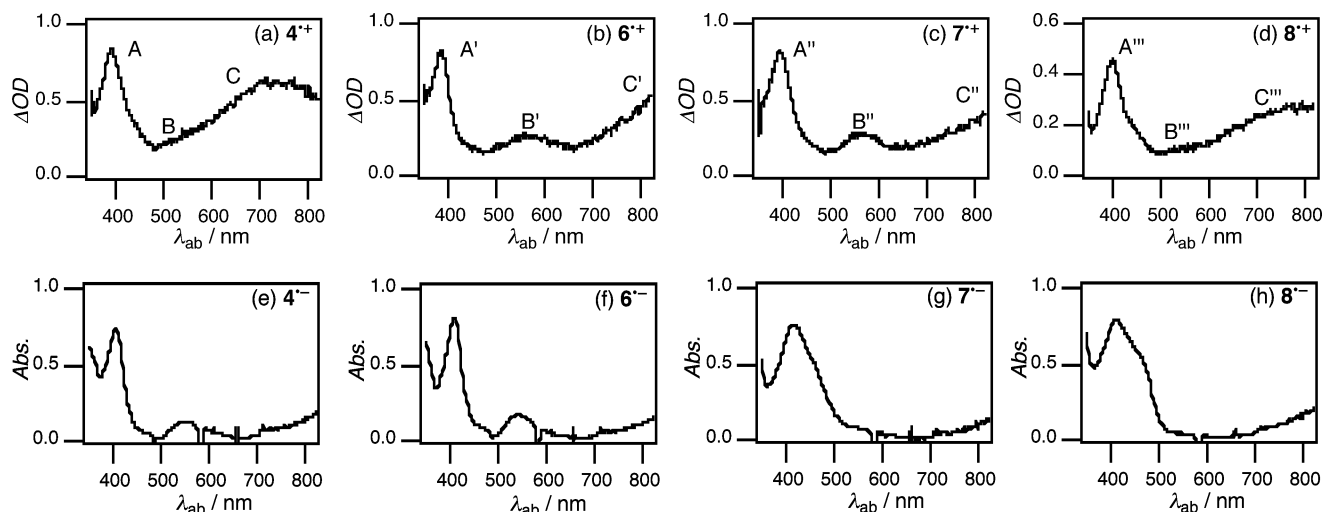


Figure 1. (a)–(d) Nanosecond time-resolved UV/vis absorption spectra observed 100 ns following the laser pulse on LFP of **4** and **6–8** (1 mM) and (e)–(f) UV/vis absorption spectra observed after γ -irradiation in 2-methyltetrahydrofuran glassy matrices of **4** and **6–8** (5 mM) at 77 K.

The sample solution was irradiated with 10 ns pulse beams obtained from a YAG laser system (Continuum Surelite-10, Nd, THG, $\lambda_{\text{ex}} = 355$ nm, 55 mJ) under air. The probe assembly consisted of a monitoring lamp (Xe arc lamp, 150 W), a polychromator equipped with an image-intensifier coupled with an image sensor, and a personal computer. The monitoring beam was adjusted so that it was perpendicular to the excitation pulse.

Measuring the UV/Vis Absorption Spectrum of a γ -Irradiated Glassy Matrix. A solution of *n*-butyl chloride or 2-methyltetrahydrofuran (1 mL) containing substrate (5 mM) in a flat vessel (synthetic quartz, $2 \times 10 \times 40$ mm thickness \times width \times height) was degassed by five freeze (77 K)–pump (10^{-2} Torr)–thaw (ambient temperature) cycles and then sealed at 10^{-2} Torr. A glassy matrix was obtained by steeping the vessel in liquid nitrogen. This vessel was irradiated with γ -rays from a 4.0 TBq ^{60}Co source in liquid N_2 at 77 K for 40 h at the Cobalt 60 γ Ray Irradiation Facility, Tohoku University. The changes in the absorption spectra between before and after irradiation were observed at 77 K with an absorption spectrophotometer.

Quantum Chemical Calculations. The geometries of the radical cations, radical anions, and radicals were optimized at the unrestricted B3LYP [Becke’s hybrid, three-parameter functional¹⁷ and the nonlocal correlation functional of Lee, Yang, and Parr (B3LYP)¹⁸ level with the standard cc-pVDZ or the aug-cc-pVDZ basis set. Vibrational analyses confirmed a DFT stationary point as energy minima (no imaginary frequencies). Wavefunction analyses for charge and spin density distributions used the conventional Mulliken partitioning scheme.²⁰ Spin contamination is negligible ($\langle s^2 \rangle = 0.7500$ – 0.7501) for the radical cations and radical anions of **4**, **6**, **7**, and **8**. Excitation energies were computed using TD-DFT (TD-B3LYP) with the cc-pVDZ basis set. DFT calculations for them and related species ($\mathbf{1}^-$, $\mathbf{1}^\bullet$, and $\mathbf{1}^+$), were carried out with the Gaussian 98 programs²¹ using extended basis sets, including d-type polarization functions on carbon. Figures 4 and 5 were drawn using MolStudio software.²²

It is reported that Møller–Plesset perturbation theory (MP2) overestimates spin densities on carbon significantly for some systems.²³ On the other hand, DFT methods²⁴ often give satisfactory results. Stephens and co-workers reported¹⁹ that the DFT/B3LYP force field gave satisfactory results of the vibrational absorption and circular dichroism spectra, as compared with the SCF or MP2 force field. Indeed, in our experience,

TABLE 1: Experimental Absorption Wavelengths (λ_{ab}) Observed on LFP and on γ -Irradiation of Low-Temperature Matrices and the Calculated Electronic Transition Wavelengths (λ_{et}) for the Radical Cations and Radical Anions of **4 and **6–8****

species	λ_{ab} , nm			λ_{et} , nm		
4 ⁺	391 (A)	480–580 (B)	>600 (C)	362	506	751
6 ⁺	386 (A')	500–650 (B')	>700 (C')	353	554	780
7 ⁺	394 (A'')	500–650 (B'')	>700 (C'')	360	557	779
8 ⁺	399 (A''')	480–580 (B''')	>600 (C''')	370	510	746
4 ⁻	408			385		
6 ⁻	406			380		
7 ⁻	416			398		
8 ⁻	412			431		

positive charge and spin densities calculated with the DFT/B3LYP method are good enough to explain the reactivity of 2,2',3,3'-tetraphenylbicyclopropenyls radical cation [ROB3LYP/6-31G(p)],²⁵ the molecular geometry and electronic structure of the geminally diphenyl-substituted trimethylenemethane (TMM) radical cations (UB3LYP/cc-pVDZ)²⁶ and 1,4-diphenylcyclohexane-1,4-diyl radical (UB3LYP/cc-pVDZ),²⁷ and others.²⁸

Results

UV/Vis Absorption Spectroscopy of Radical Cations. If **4**⁺ and related radical cations have a nonclassical nature, as proposed by Hirano and Ohashi, this must be reflected in their UV/vis absorption spectra.

First, nanosecond time-resolved UV/vis absorption spectroscopy on LFP was performed using $\text{NMQ}^+\text{BF}_4^-$ ²⁹ as a sensitizer and toluene as a cosensitizer,³¹ in aerated acetonitrile at 298 K. As shown in Figure 1a–d and summarized in Table 1, laser excitation (355 nm) of $\text{NMQ}^+\text{BF}_4^-$ with **4**, **6**, **7**, and **8** in aerated acetonitrile produced characteristic absorption bands, each of which can be assigned to the appropriate radical cation. Radical cation **4**⁺ exhibited an intense, sharp absorption band with λ_{ab} at 391 nm (band A), a broad, weak absorption band at 480–580 nm (band B), and a broad, intense absorption band at >600 nm (band C) (Figure 1a). Similarly, **6**⁺ and **7**⁺ displayed intense, sharp absorption bands with λ_{ab} at 386 (band A') and 394 nm (band A''), respectively, a broad, weak absorption band at 500–650 nm (band B' for **6**⁺ and B'' for **7**⁺), and a broad, intense absorption band at >700 nm (band C' for **6**⁺ and C'' for **7**⁺) (Figure 1b,c). Radical cation **8**⁺, a hybrid of **4**⁺ and

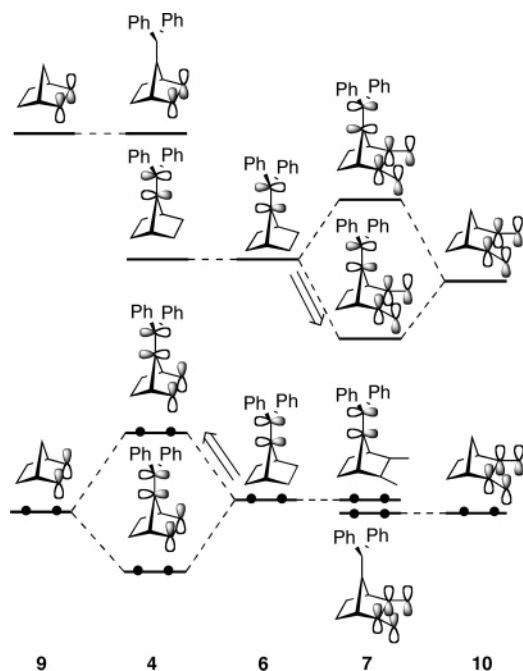


Figure 2. MOs involved in electronic coupling in **4** and **7** derived from **6**, **9**, and **10**. Thick arrows indicate the lowering of the LUMO level of **7** and the increase of the HOMO level of **4** compared with **6**.

7⁺, had an intense, sharp absorption band with λ_{ab} at 399 nm (band A'''), a broad, weak absorption band at 480–580 nm (band B'''), and a broad, intense absorption band at >600 nm (band C''') (Figure 1d).

Bands A, A', A'', and A''' of **4**⁺, **6**⁺, **7**⁺, and **8**⁺ exhibited different values for λ_{ab} . Note that the bands A, A', and A''' of **4**⁺, **7**⁺, and **8**⁺, respectively, which have *p*-orbitals at C-2 and C-3 in common, shifted to slightly longer wavelengths when compared with band A' of **6**⁺. In the visible region, bands B and C of **4**⁺ and bands B''' and C''' of **8**⁺ arise in a similar manner and, by analogy, bands B' and C' of **6**⁺ closely resemble bands B'' and C'' of **7**⁺, respectively.

UV/Vis Absorption Spectroscopy of Radical Anions. Our attempts to examine the radical anions of **4**, **6**, **7**, and **8** were frustrated when we were unable to generate **4**⁻, **6**⁻, **7**⁻, or **8**⁻ under PET conditions because of the lack of suitable electron-donor photosensitizers. Consequently, we adopted a procedure involving γ -irradiation of low-temperature 2-methyltetrahydrofuran glassy matrices^{32,33} that contained **4**, **6**, **7**, and **8**. As shown in Figure 1e–h and summarized in Table 1, **4**⁻,³⁴ **6**⁻,³⁴ **7**⁻, and **8**⁻ possessed intense absorption bands with λ_{ab} at 408, 406, 416, and 412 nm, respectively. Both **7**⁻ and **8**⁻, which contain 1,3-butadiene subunits, exhibited broad absorption bands, and **4**⁻ and **6**⁻ displayed sharp absorption bands.

Discussion

Elucidation of the Molecular Orbitals (MOs) of Neutral Precursors using Orbital Interaction (OI) Theory. Figure 2 presents a graphical model of electronic coupling in neutral precursors **4** and **7**. The MOs of **4** are derived from those of the ethylene subunits of **6** and norbornene (**9**), and the MOs of the ethylene and 1,3-butadiene subunits of **6** and 2,3-dimethylenenorbornane (**10**) represent those of **7**. The HOMOs of **6** and **9** are allowed to interact with each other efficiently to yield the HOMO of **4** having an antibonding character, because the three orbitals at C-7 of **6** and at C-2 and C-3 of **9** are in phase with each other.³⁵ Conversely, any electronic coupling between the

LUMOs of **6** and **9** is impossible because of the topological disagreement of the orbitals at C-7 of **6** and at C-2 and C-3 in **9**. Similarly, potential electronic coupling between the HOMOs of **6** and **10** is negated by the topological disagreement of the orbitals at C-7 of **6** and at C-2 and C-3 of **10**. Therefore, the HOMO of **7** corresponds to that of **6**. Note that the LUMOs of **6** and **10** are able to interact with each other to give the LUMO of **7** that possesses a bonding character as a consequence of the orbitals at C-7 in **6** and at C-2 and C-3 in **10** being in phase. Consequently, electronic coupling causes a rise in the HOMO level of **4** and a lowering of the LUMO level of **7** when compared with those of **6**, but the LUMO level of **4** and the HOMO level of **7** change little.

As noted above, **8** should contain aspects of the natures of both **4** and **7**, with the HOMO and LUMO levels of **8** predicted to correspond with those of **4** and **7** in their antibonding and bonding characters, respectively, as a result of an effective OI in both the HOMO and LUMO.

The MOs of radical cations and radical anions have been taken to approximate those of the neutral precursors shown in Figure 2, allowing for the simple ejection or injection of an electron. Because the HOMOs and LUMOs of the neutral precursors will correspond to the singly occupied MOs (SOMOs) of radical cations and radical anions, respectively, the ejection of an electron from the HOMO of **4** will induce a decreasing repulsive interaction among C-2, C-3, and C-7 in the resulting **4**⁺, but will not induce an increasing attractive interaction. In contrast, the injection of an electron into the LUMO of **7** will induce an increasing attractive interaction in **7**⁻.

TD-DFT Calculations. TD-DFT calculations were used to evaluate the observed spectroscopic behavior. The electronic transition wavelengths (λ_{et}) and oscillator strengths (*f*) of **4**⁺, **6**⁺, **7**⁺, and **8**⁺ in the optimized structures (vide infra) were calculated with TD-UB3LYP/cc-pVDZ (Figure 3a–d and Table 1). The calculations gave λ_{et} at 362, 506, and 751 nm with *f* = 0.187, 0.009, and 0.087 for **4**⁺, λ_{et} at 353, 554, and 780 nm with *f* = 0.153, 0.027, and 0.094 for **6**⁺, λ_{et} at 360, 557, and 779 nm with *f* = 0.196, 0.042, and 0.089 for **7**⁺, and λ_{et} at 370, 510, and 746 nm with *f* = 0.225, 0.027, and 0.078 for **8**⁺, respectively. These calculated electronic transitions successfully reproduced the observed red and blue shifts of the λ_{ab} of **4**⁺, **7**⁺ and **8**⁺ as compared with those of **6**⁺ (Figure 1a–d).

An analysis based on the TD-UB3LYP/cc-pVDZ calculations suggests that bands A, A', A'', and A''' of **4**⁺, **6**⁺, **7**⁺, and **8**⁺ originate from SOMO → LUMO transitions, whereas bands C, C', C'', and C''' arise from SOMO-*X* → LUMO transitions (*X* = 4, 3, 4, and 5 for **4**⁺, **6**⁺, **7**⁺, and **8**⁺, respectively). Figure 4 provides a schematic representation of the MOs associated with the calculated transitions for bands A, A', A'', and A''' and bands C, C', C'', and C''' of **4**⁺, **6**⁺, **7**⁺, and **8**⁺, respectively. For convenience, the representations of SOMO-*X*, SOMO, and LUMO for **4**⁺, **6**⁺, **7**⁺, and **8**⁺ have been replaced with the corresponding HOMO-*X*, HOMO, and LUMO of the neutral molecules **4**, **6**, **7**, and **8**, calculated using RB3LYP/cc-pVDZ. Note that each SOMO-*X* possesses a similar type of MO with orbital coefficients at the atoms of the benzhydrylidene subunits only, and that the distribution patterns of the orbital coefficients of the SOMOs and LUMOs are in line with those shown in Figure 2. Therefore, the observed red and blue shifts of the absorption bands of **4**⁺, **6**⁺, **7**⁺, and **8**⁺ can be clearly explained in terms of changes in the energy levels of the MOs induced by electronic coupling among C-2, C-3, and C-7, as outlined above.

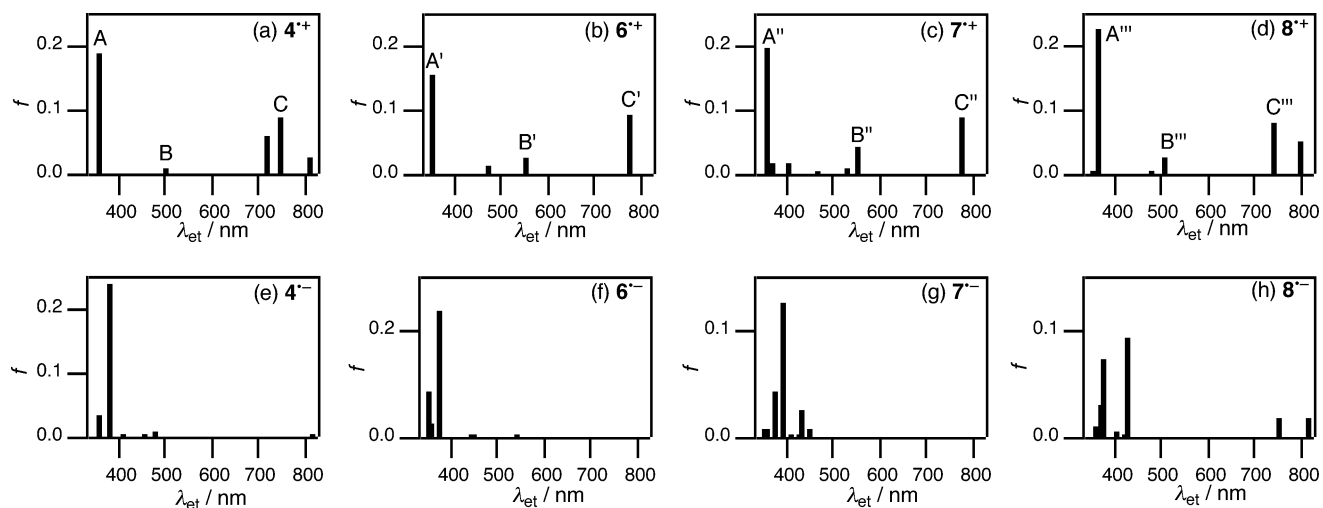


Figure 3. Electronic transitions of the radical cations (a)–(d) and radical anions (e)–(h) of **4** and **6–8** calculated using TD-UB3LYP/cc-pVDZ.

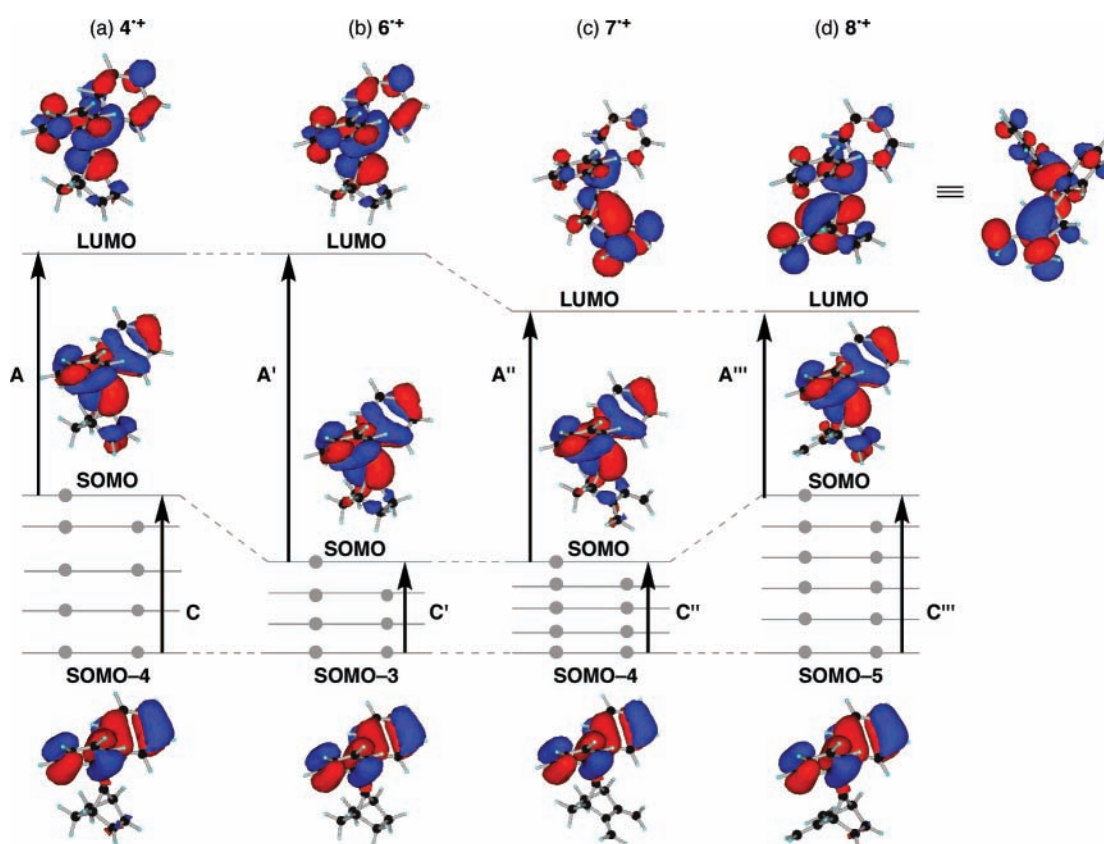


Figure 4. MOs of the radical cations of **4** and **6–8** (a)–(d) associated with bands A, A', A'', and A''' and C, C', C'', and C'''.

The shift pattern of the absorption bands of $8^{\bullet+}$ is of some interest. The hybrid radical cation $8^{\bullet+}$ has the smallest SOMO–LUMO gap a result of the increase in the SOMO coincident with a lowering of the LUMO levels when compared with those of $6^{\bullet+}$. Consequently, band A''' in $8^{\bullet+}$ occurs at a longer wavelength than bands A, A', and A'' of $4^{\bullet+}$, $6^{\bullet+}$, and $7^{\bullet+}$. However, because band C''' of $8^{\bullet+}$ arises from the SOMO-5 \rightarrow SOMO transition, whose energy gap is comparable to that of the SOMO-4 \rightarrow SOMO transition of $4^{\bullet+}$, then band C''' of $8^{\bullet+}$ is predicted to behave similarly to band C of $4^{\bullet+}$ and, indeed, the experimental results show a very high level of consistency with the theoretical calculations for the radical cation system of the 7-benzhydrylidenenorbornene derivatives.

Similarly, the TD-UB3LYP/cc-pVDZ calculations for the optimized structures (vide infra) of $4^{\bullet-}$, $6^{\bullet-}$, $7^{\bullet-}$, and $8^{\bullet-}$, as

shown in Figure 3e–h and summarized in Table 1, gave λ_{et} at 385 nm with $f = 0.239$ for $4^{\bullet-}$, λ_{et} at 380 nm with $f = 0.235$ for $6^{\bullet-}$, λ_{et} at 398 nm with $f = 0.125$ for $7^{\bullet-}$, and λ_{et} at 431 nm with $f = 0.091$ for $8^{\bullet-}$. These λ_{et} are mainly due to HOMO \rightarrow SOMO electronic transitions, with the HOMOs and SOMOs of $4^{\bullet-}$, $6^{\bullet-}$, $7^{\bullet-}$, and $8^{\bullet-}$ corresponding to the SOMOs and LUMOs of $4^{\bullet+}$, $6^{\bullet+}$, $7^{\bullet+}$, and $8^{\bullet+}$, respectively (Figure 4). The absorption bands of $4^{\bullet-}$, $6^{\bullet-}$, $7^{\bullet-}$, and $8^{\bullet-}$ correspond to bands A, A', A'', and A''' of $4^{\bullet+}$, $6^{\bullet+}$, $7^{\bullet+}$, and $8^{\bullet+}$, respectively; therefore, the red shifts observed in the absorption bands of $4^{\bullet-}$ and $7^{\bullet-}$, when compared with that of $6^{\bullet-}$, can reasonably be described in terms of MOs and reproduced successfully using TD-DFT calculations. Unfortunately, the calculated result for $8^{\bullet-}$ conflicts with the observed behavior. An excellent agreement of the pattern of absorptions for $8^{\bullet-}$ with that of electronic transitions indicates

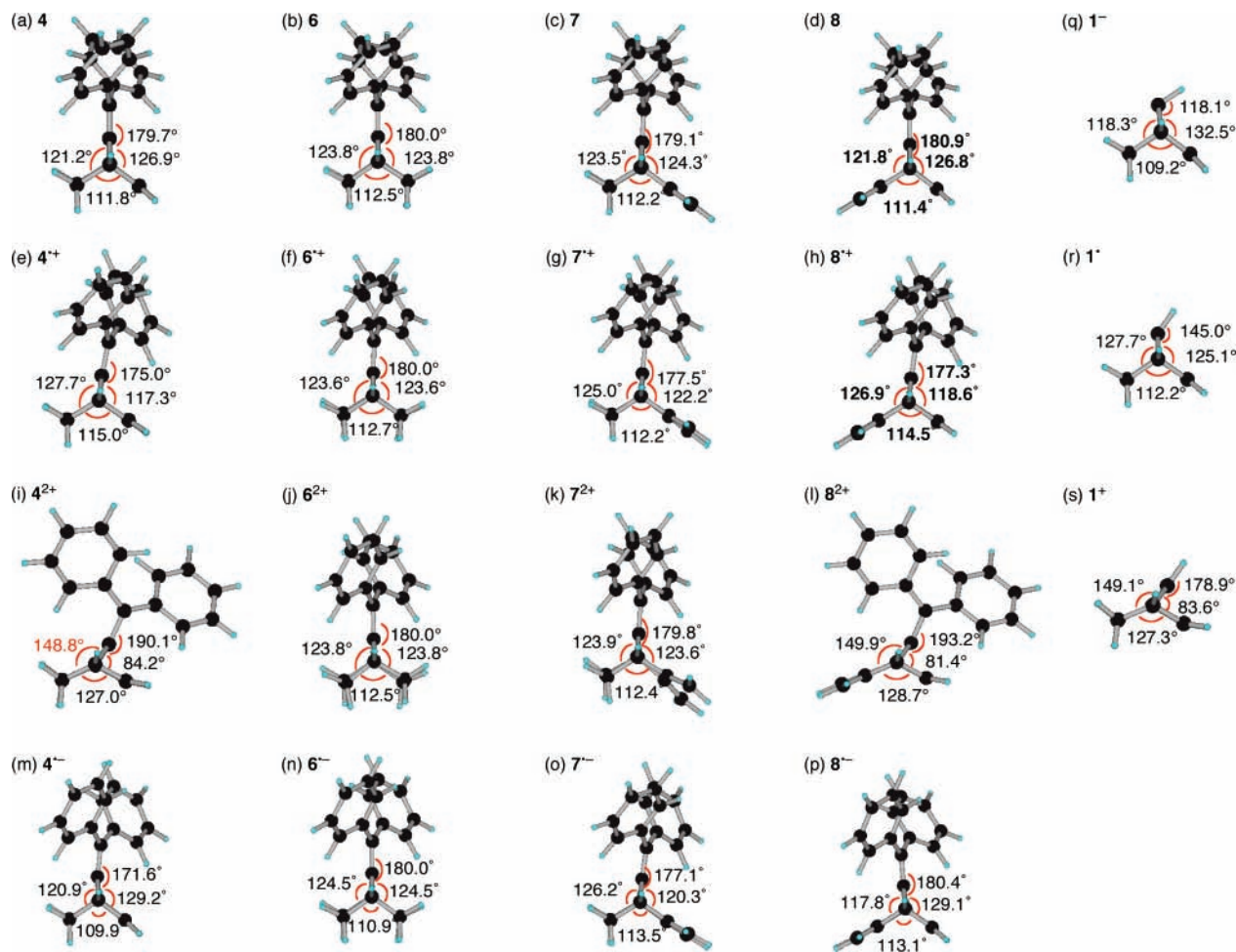


Figure 5. Side views of neutral (a)–(d), radical cation (e)–(h), dication (i)–(l), and radical anion (m)–(p) species of **4** and **6–8** and **1⁻** (q), **1⁺** (r), and **1⁺** (s) optimized using the (U)B3LYP/(aug-)cc-pVDZ calculations.

the adequacy of the TD-DFT calculation. On the other hand, from the TD-DFT calculation, the absorption band of **8⁻** would occur at the longest wavelength among those found for **4⁻**, **6⁻**, and **7⁻**. In fact, the observed band for **8⁻** is shifted to a wavelength shorter than that of **7⁻**. At present, we are unable to explain this result, although higher-level MO calculations might resolve the issue.

Geometry Optimization Using DFT Calculations. DFT calculations were used to provide insight into the molecular geometry. In Figure 5a–d, the C-1–C-7–C-4 skeletons of neutral **4**, **7**, and **8** are bent slightly toward the C-5–C-6 side, whereas **6** possesses a symmetrical molecular geometry at the RB3LYP/cc-pVDZ level of theory. Interestingly, the C-1–C-7–C-4 skeletons of **4⁺** and **8⁺** bend toward the C-2–C-3 side with a magnitude that is larger than in either **6⁺** or **7⁺** (Figure 5e–h). At the UB3LYP/cc-pVDZ level, the magnitude of the bent structure of the C-1–C-7–C-4 skeletons to C-2–C-3 is 5.2° [= (360.0° – 115.0°)/2 – 117.3°] for **4⁺** and 4.2° [= (360.0° – 114.5°)/2 – 118.6°] for **8⁺**. Although this result is consistent with the nonclassical nature of the radical cation,⁹ the magnitude of the bend is somewhat smaller than might be anticipated from the observed π -facial selectivity under PET conditions (Scheme 1). The bend in the C-1–C-7–C-4 skeleton of nonclassical cation **1⁺** toward the C-2–C-3 side can be calculated as 32.8° [= (360.0° – 127.3°)/2 – 83.6°] at the RB3LYP/cc-pVDZ level (Figure 5s). As shown in Figure 6, the bent structure of **1⁺** can be explained by the attractive force among C-2, C-3, and C-7 induced by the presence of two electrons in the HOMO with a bonding character, with any

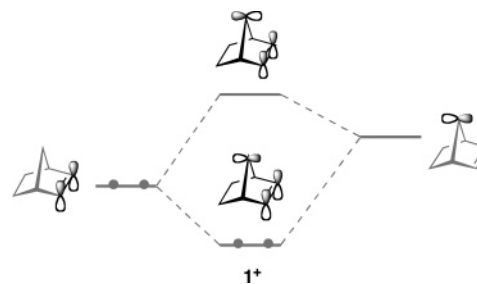


Figure 6. OI of **1⁺** among the *p*-orbitals at C-2, C-3, and C-7.

potential repulsive forces absent, as no electron exists in the LUMO with an antibonding character. In contrast, in **4⁺** and **8⁺**, repulsive forces are active among C-2, C-3, and C-7 due to the presence of an electron in the SOMO with an antibonding character (Figure 4). For this reason, the structures of **4⁺** and **8⁺** will be less bent than that of **1⁺**. The hypothetical dications **4²⁺** and **8²⁺**, which have no electrons in an antibonding MO, are bent even more significantly as much as **1⁺** (Figure 5i and 5l). Note that **6⁺**, **7⁺**, **6²⁺**, and **7²⁺** do not have bent structures (Figure 5f,g,j,k) because their SOMOs or HOMOs having a nonbonding character. These results strongly point to strong electronic coupling among C-2, C-3, and C-7 in the HOMO in **4** and **8**, but its absence in **6** and **7**. These results are consistent with those obtained using OI theory and are indicative of the nonclassical nature of **4⁺** and **8⁺**. In this sense, the neutral, radical cation, and dication states of 7-benzhydrylidenebornene derivatives correspond with **1⁻**, **1⁺**, and **1⁺**, respectively.

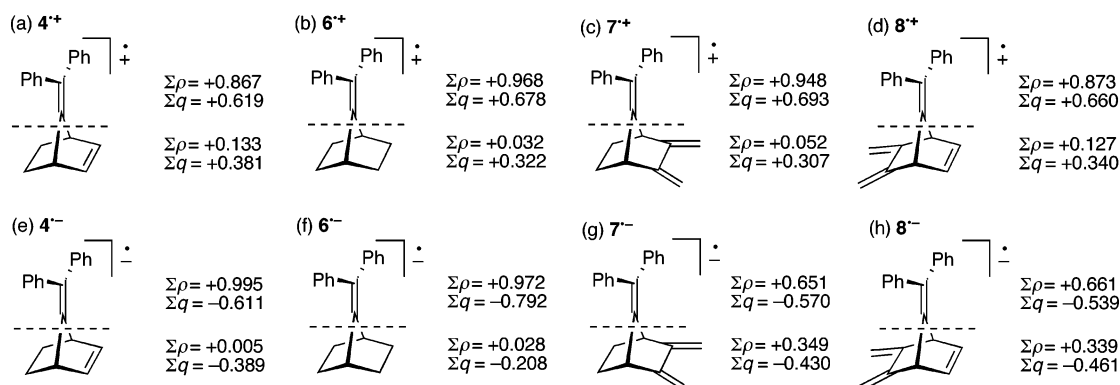


Figure 7. Sum of the partial spin (ρ) and charge (q) densities of the benzhydrylidene subunit and residual subunit in radical cations (a)–(d) and radical anions (e)–(h) of **4** and **6–8** calculated using UB3LYP/cc-pVDZ.

On the basis of the concepts outlined above, it is anticipated that $7^{\bullet-}$ and $8^{\bullet-}$ have a nonclassical nature with bent structures induced by the presence of an electron in their SOMO having a bonding character, whereas $4^{\bullet-}$ and $6^{\bullet-}$ have a classical nature and nonbent structures because of a SOMO with a nonbonding character. Essentially, DFT calculations at the UB3LYP/cc-pVDZ level point to the C-1–C-7–C-4 skeletons of $7^{\bullet-}$ and $8^{\bullet-}$ being bent to the side of the C-2–C-3 and C-5–C-6 subunit by 3.0° [$=(360.0^\circ - 113.5^\circ)/2 - 120.3^\circ$] and 5.7° [$=(360.0^\circ - 113.1^\circ)/2 - 117.8^\circ$], respectively, whereas $4^{\bullet-}$ and $6^{\bullet-}$ lack such structures (Figure 5m–p). Although $8^{+\bullet}$ is bent to the C-2–C-3 side, $8^{\bullet-}$ bends to the C-5–C-6 side, reflecting the hybrid character of **4** and **7**.

The sum of partial spin (ρ) and charge (q) densities, $\Sigma\rho$ and Σq , computed from DFT calculations,³⁶ are shown in Figure 7 and provide insight into the electronic structure. The values, $\Sigma\rho = +0.867$ and $\Sigma q = +0.619$, of the benzhydrylidene subunit in $4^{+\bullet}$ are less than those of $6^{+\bullet}$, which are $+0.968$ and $+0.678$, respectively. Consequently, the corresponding values of the residual subunit of $+0.133$ and $+0.381$ are greater than those of $6^{+\bullet}$ of $+0.032$ and $+0.322$. The spin and charge distributions of $4^{+\bullet}$ resemble those of $8^{+\bullet}$ ($\Sigma\rho = +0.873$ and $\Sigma q = +0.660$ in the benzhydrylidene subunit), whereas the spin and charge distributions of $6^{+\bullet}$ are closer to those of $7^{+\bullet}$ ($\Sigma\rho = +0.948$ and $\Sigma q = +0.693$). These results are consistent with the nonclassical nature of $4^{+\bullet}$ and $8^{+\bullet}$, whose spin and positive charge are delocalized not only in the benzhydrylidene subunit but also in the residual subunit, and with the classical nature of $6^{+\bullet}$ and $7^{+\bullet}$, whose spin and positive charge are localized mainly in the benzhydrylidene subunit.

In the radical anion system, the spin and charge distributions of $4^{\bullet-}$ ($\Sigma\rho = +0.995$ and $\Sigma q = -0.611$ in the benzhydrylidene subunit) resemble those of $6^{\bullet-}$ ($\Sigma\rho = +0.972$ and $\Sigma q = -0.792$), whereas the spin and charge distributions of $7^{\bullet-}$ ($\Sigma\rho = +0.651$ and $\Sigma q = -0.570$) more closely resemble those of $8^{\bullet-}$ ($\Sigma\rho = +0.661$ and $\Sigma q = -0.539$). Furthermore, both the spin and charge of $7^{\bullet-}$ and $8^{\bullet-}$ are delocalized, not only in the benzhydrylidene subunit, but also in the residual subunit, when compared with those of $4^{\bullet-}$ and $6^{\bullet-}$. Again, these results affirm the nonclassical nature of $7^{\bullet-}$ and $8^{\bullet-}$ and the classical nature of $4^{\bullet-}$ and $6^{\bullet-}$.

All these results correspond with the structure optimized using DFT calculations and account for the strong similarities in the experimental spectra between $4^{+\bullet}$ and $8^{+\bullet}$, $6^{+\bullet}$ and $7^{+\bullet}$, $4^{\bullet-}$ and $6^{\bullet-}$, and $7^{\bullet-}$ and $8^{\bullet-}$.

Conclusion

Spectroscopic and DFT calculation studies enabled us to confirm the contrasting nonclassical and classical natures of

radical cations and radical anions. Especially, we are the first to demonstrate the nonclassical nature of radical anions. DFT calculations demonstrate that the radical cations $4^{+\bullet}$ and $8^{+\bullet}$ and radical anions $7^{\bullet-}$ and $8^{\bullet-}$ have a nonclassical nature with a bent structure and delocalized electronic state, whereas the radical cations $6^{+\bullet}$ and $7^{+\bullet}$ and radical anions $4^{\bullet-}$ and $6^{\bullet-}$ have a classical nature with a nonbent structure and localized electronic state. These differences in molecular geometry and electronic structure are clearly reflected in the red and blue shifts and in the shapes of the absorption bands in UV/vis absorption spectra, which are reproduced successfully by the TD-DFT calculations. Further, changes in the absorption bands can be accounted for by OI theory. The contrasting nonclassical and classical natures can be attributed to differences in the pattern of their electronic coupling. In particular, the topological agreement and disagreement of the orbitals at C-2, C-3 (or C-5, C-6), and C-7 strongly control the nature of the radical ions in the 7-benzhydrylidenenorbornene system. From the viewpoint of MOs, the neutral, radical cation, and dication states of the 7-benzhydrylidenenorbornene derivatives correspond to the anion, radical, and cation states of 7-norbornenyl, respectively. Our results provide meaningful information, not only for the pure radical ion chemistry of the organic compounds but also for the application of molecular design in new redox systems containing topological characteristics.

Acknowledgment. H.I. and K.M. gratefully acknowledge financial support from a Grant-in-Aid for Scientific Research on Priority Areas (Nos. 14050008 and 17029058 in Area No. 417) and others (Nos. 16655018, 18037063, and 19350025) from the Ministry of Education, Culture, Sports, Science, and Technology of Japan. H.I. gratefully acknowledges the Izumi Science and Technology Foundation, the Shorai Foundation, and the Iketani Foundation for Science and Technology. We also thank Professors M. Ueda (TU) and H. Niwa (UEC) and Emeritus Professor M. Ohashi (UEC) for their generous assistance, Professor S. Koseki (OPU) for his valuable discussion, and the late Mr. S. Shiina (UEC) for his effort in preparing the samples.

Supporting Information Available: General methods of the experiments, preparation of **4**, **6**, **7**, and **8**, the DFT calculation results (Cartesian coordinates, Mulliken spin and charge densities) of **4**, 4^{2+} , $4^{\bullet-}$, **6**, $6^{+\bullet}$, 6^{2+} , $6^{\bullet-}$, **7**, $7^{+\bullet}$, 7^{2+} , $7^{\bullet-}$, **8**, $8^{+\bullet}$, 8^{2+} , $8^{\bullet-}$, **1**⁻, **1**[•], and **1**⁺ optimized using DFT calculations, and the definition of angles. This material is available free of charge via the Internet at <http://pubs.acs.org>.

References and Notes

- (1) March, J. In *Advanced Organic Chemistry, Reactions, Mechanisms, and Structure*, 3rd ed.; Wiley: New York, 1985; pp 272–287 and references cited therein.
- (2) (a) Winstein, S. In *Carbonium Ions*; Olah, G. A., Schleyer, P. v. R., Eds.; Wiley: New York, 1972; Vol. 3, pp 965–1006.
- (3) (a) Winstein, S.; Shatavsky, M.; Norton, C.; Woodward, R. B. *J. Am. Chem. Soc.* **1955**, *77*, 4183–4184. (b) Winstein, S.; Stafford, E. T. *J. Am. Chem. Soc.* **1957**, *79*, 505–506.
- (4) See also: (a) Woods, W. G.; Carboni, R. A.; Roberts, J. D. *J. Am. Chem. Soc.* **1956**, *78*, 5653–5657. (b) Woods, W. G.; Carboni, R. A.; Roberts, J. D. *J. Am. Chem. Soc.* **1962**, *84*, 4876–4882.
- (5) Brown, H. C.; Bell, H. M. *J. Am. Chem. Soc.* **1963**, *85*, 2324.
- (6) (a) Olah, G. A.; Liang, G. *J. Am. Chem. Soc.* **1975**, *97*, 6803–6806. (b) Lustgarten, R. K.; Brookhart, M.; Winstein, S.; Gassman, P. G.; Patton, D. S.; Richey, H. G., Jr.; Nicholas, J. D. *Tetrahedron Lett.* **1970**, *11*, 1699–1702.
- (7) (a) Houriet, R.; Schwitzguebel, T.; Carrupt, P.-A.; Vogel, P. *Tetrahedron Lett.* **1986**, *27*, 37–40. (b) Bremer, M.; Schotz, K.; Schleyer, P. v. R.; Fleischer, U.; Schindler, M.; Kutzelnigg, W.; Koch, W.; Pulay, P. *Angew. Chem., Int. Ed. Engl.* **1989**, *28*, 1042–1044.
- (8) (a) Laube, T. *J. Am. Chem. Soc.* **1989**, *111*, 9224–9232. (b) Laube, T. *Acc. Chem. Res.* **1995**, *28*, 399–405. (c) Laube, T. *J. Am. Chem. Soc.* **2004**, *126*, 10904–10912.
- (9) (a) Roth, H. D.; Du, X.-M.; Weng, H.; Lakkaraju, P. S.; Abelt, C. *J. Am. Chem. Soc.* **1994**, *116*, 7744–7752. (b) Weng, H.; Du, X.-M.; Roth, H. D. *J. Am. Chem. Soc.* **1995**, *117*, 135–140.
- (10) The anodic peak potential ($E_{1/2}^{ox}$) of **4** is +1.50 V vs SCE in acetonitrile. See ref 11.
- (11) (a) Hirano, T.; Shiina, S.; Ohashi, M. *J. Chem. Soc., Chem. Commun.* **1992**, 1544–1546. (b) Ishii, H.; Shiina, S.; Hirano, T.; Niwa, H.; Ohashi, M. *Tetrahedron Lett.* **1999**, *40*, 523–526.
- (12) As one of the referee suggested, the “classical/nonclassical” designation is originally limited to carbocations. In this and related papers (refs 14a and 14b), however, the authors take this designation in the broad sense, similar to the case of “a contact/separated ion pair”. This word was used for intermediates in solvolysis at first, but now used for those of electron-transfer reactions, too.
- (13) For suggestions of similar electronic coupling in reactive radical cations, see ref 14.
- (14) (a) Ikeda, H.; Tanaka, F.; Kabuto, C. *Tetrahedron Lett.* **2005**, *46*, 2663–2667. (b) Ikeda, H.; Hoshi, Y.; Kikuchi, Y.; Tanaka, F.; Miyashi, T. *Org. Lett.* **2004**, *6*, 1029–1032. (c) Ikeda, H.; Hoshi, Y.; Miyashi, T. *Tetrahedron Lett.* **2001**, *42*, 8485–8488. (d) Ikeda, H.; Takasaki, T.; Takahashi, Y.; Konno, A.; Matsumoto, M.; Hoshi, Y.; Aoki, T.; Suzuki, T.; Goodman, J. L.; Miyashi, T. *J. Org. Chem.* **1999**, *64*, 1640–1649. (e) Ikeda, H.; Minegishi, T.; Abe, H.; Konno, A.; Goodman, J. L.; Miyashi, T. *J. Am. Chem. Soc.* **1998**, *120*, 87–95. (f) Brede, O.; David, F.; Steenken, S. *J. Chem. Soc., Perkin Trans. 2* **1995**, 23–32. (g) Williams, F. *J. Chem. Soc., Faraday Trans.* **1994**, *90*, 1681–1687. (h) Tamai, T.; Mizuno, K.; Hashida, I.; Otsuji, Y. *J. Org. Chem.* **1992**, *57*, 5338–5342. (i) Tojo, S.; Toki, S.; Takamuku, S. *J. Org. Chem.* **1991**, *56*, 6240–6243. (j) Pac, C. *Pure Appl. Chem.* **1986**, *58*, 1249–1256.
- (15) Part of this work was reported as a preliminary communication, see: (a) Ikeda, H.; Namai, H.; Hirano, T. *Tetrahedron Lett.* **2005**, *46*, 3917–3921. (b) Ikeda, H.; Namai, H.; Hirano, T. *Tetrahedron Lett.* **2005**, *46*, 7631–7635.
- (16) De Lucchi, O.; Lucchini, V.; Pasquato, L.; Modena, G. *J. Org. Chem.* **1984**, *49*, 596–604.
- (17) Becke, A. D. *J. Chem. Phys.* **1993**, *98*, 5648–5652.
- (18) Lee, C.; Yang, W.; Parr, R. G. *Phys. Rev. B* **1988**, *37*, 785–789.
- (19) Stephens, P. J.; Devlin, F. J.; Chabalowski, C. F.; Frisch, M. J. *J. Phys. Chem.* **1994**, *98*, 11623–11627.
- (20) Mulliken, R. S. *J. Chem. Phys.* **1955**, *23*, 1833–1840.
- (21) Frisch, M. J.; Trucks, G. W.; Schlegel, H. B.; Scuseria, G. E.; Robb, M. A.; Cheeseman, J. R.; Zakrzewski, V. G.; Montgomery, J. A.; Stratmann, R. E.; Burant, J. C.; Dapprich, S.; Millam, J. M.; Daniels, A. D.; Kudin, K. N.; Strain, M. C.; Farkas, O.; Tomasi, J.; Barone, V.; Cossi, M.; Cammi, R.; Mennucci, B.; Pomelli, C.; Adamo, C.; Clifford, S.; Ochterski, J.; Petersson, G. A.; Ayala, P. Y.; Cui, Q.; Morokuma, K.; Malick, D. K.; Rabuck, A. D.; Raghavachari, K.; Foresman, J. B.; Cioslowski, J.; Ortiz, J. V.; Stefanov, B. B.; Liu, G.; Liashenko, A.; Piskorz, P.; Komaromi, I.; Gomperts, R.; Martin, R. L.; Fox, D. J.; Keith, T.; Al-Laham, M. A.; Peng, C. Y.; Nanayakkara, A.; Gonzalez, C.; Challacombe, M.; Gill, P. M. W.; Johnson, B. G.; Chen, W.; Wong, M. W.; Andres, J. L.; Head-Gordon, M.; Replogle, E. S.; Pople, J. A. *Gaussian 98*, revision A.11.4; Gaussian, Inc.: Pittsburgh, PA, 1998.
- (22) For MolStudio (NEC), visit the web site at http://www.sw.nec.co.jp/APSOFT/SX/molstudio_e/index.html.
- (23) (a) Raghavachari, K.; Haddon, R. C.; Roth, H. D. *J. Am. Chem. Soc.* **1983**, *105*, 3110–3114. (b) Raghavachari, K.; Roth, H. D. *J. Am. Chem. Soc.* **1989**, *111*, 7132–7136. (c) Roth, H. D.; Schilling, M. L. M.; Raghavachari, K. *J. Am. Chem. Soc.* **1984**, *106*, 253–255. (d) Krogh-Jespersen, K.; Roth, H. D. *J. Am. Chem. Soc.* **1992**, *114*, 8388–8394.
- (24) (a) Eriksson, L. A.; Malkin, V. G.; Malkina, O. L.; Salahub, D. R. *J. Chem. Phys.* **1993**, *99*, 9756–9763. (b) Eriksson, L. A.; Malkin, V. G.; Malkina, O. L.; Salahub, D. R. *Int. J. Quantum Chem.* **1994**, *52*, 879–901.
- (25) Ikeda, H.; Hoshi, Y.; Kikuchi, Y.; Tanaka, F.; Miyashi, T. *Org. Lett.* **2004**, *6*, 1029–1032.
- (26) Namai, H.; Ikeda, H.; Kato, N.; Mizuno, K. *J. Phys. Chem. A* **2007**, *111*, 4436–4442.
- (27) Ikeda, H.; Hoshi, Y.; Namai, H.; Tanaka, F.; Goodman, J. L.; Mizuno, K. *Chem. Eur. J.* **2007**, in press.
- (28) (a) Ikeda, H.; Tanaka, F.; Miyashi, T.; Akiyama, K.; Tero-Kubota, S. *Eur. J. Org. Chem.* **2004**, 1500–1508. (b) Ikeda, H.; Tanaka, F.; Kabuto, C. *Tetrahedron Lett.* **2005**, *46*, 2663–2667. (c) Ikeda, H.; Namai, H.; Kato, N.; Ikeda, T. *Tetrahedron Lett.* **2006**, *47*, 1501–1504. (d) Ikeda, H.; Namai, H.; Kato, N.; Ikeda, T. *Tetrahedron Lett.* **2006**, *47*, 1857–1860.
- (29) The cathodic peak potential ($E_{1/2}^{red}$) and energy of the lowest excited singlet state of $\text{NMQ}^+\text{BF}_4^-$ are -0.80 V vs SCE and 3.47 eV in acetonitrile, respectively.³⁰
- (30) Ikeda, H.; Akiyama, K.; Takahashi, Y.; Nakamura, T.; Ishizaki, S.; Shiratori, Y.; Ohaku, H.; Goodman, J. L.; Houmam, A.; Wayner, D. D. M.; Tero-Kubota, S.; Miyashi, T. *J. Am. Chem. Soc.* **2003**, *125*, 9147–9157.
- (31) The use of a cationic sensitizer and a chemically unreactive aromatic hydrocarbon, the so-called cosensitizers, in acetonitrile is effective for observing radical cations in LFP experiments. Under cosensitized conditions, a substrate radical cation is formed via electron transfer from a cosensitizer to a photoexcited sensitizer followed by hole transfer from a cosensitizer radical cation to the substrate.
- (32) 2-Methyltetrahydrofuran is a typical solvent used for generating radical anions by γ -irradiation.
- (33) Wishart, J. F.; Nocera, D. G. In *Photochemistry and Radiation Chemistry: Complementary Methods for the Study of Electron Transfer*; American Chemical Society: Washington, DC, 1998.
- (34) There are small absorption bands at 500–600 nm for $4^{\cdot-}$ and $6^{\cdot-}$. The theoretical calculation also supported them. However, we did not discuss them because these are not very important.
- (35) A similar OI was confirmed for isopropylidenebornene using photoelectron spectroscopy, see: (a) Heilbronner, E.; Martin, H.-D. *Helv. Chim. Acta* **1972**, *55*, 1490–1502. (b) Martin, H.-D.; Mayer, B. *Angew. Chem., Int. Ed. Engl.* **1983**, *22*, 283–314.
- (36) The ρ and q values for each atom are summarized in the Supporting Information.